



Eddy Current Method in Non-Magnetic Aluminide Coating Thickness Assessment

Grzegorz Tytko¹ · Małgorzata Adamczyk-Habrajska² · Yong Li³ · Shi Pengpeng⁴ · Mateusz Kopec⁵

Received: 27 February 2025 / Accepted: 2 June 2025
© The Author(s) 2025

Abstract

This study investigates the use of eddy current testing (ECT) as a non-destructive technique to evaluate the thickness and structural variations of non-magnetic aluminide coatings on MAR-M247 nickel-based superalloy. Coatings with thicknesses of 20 μm and 40 μm were applied to substrates exhibiting fine, coarse, and columnar grain structures. Using sensors of different geometries, impedance measurements were performed within a frequency range of 11.5 MHz to 12.5 MHz. Results demonstrated the designed sensor's superior sensitivity, with the highest values of absolute resistance difference significantly exceeding the threshold for reliable distinction due to coating thicknesses or grain structures. The study highlights the impact of eddy current penetration depth and edge effects on the measurement accuracy, emphasizing the need for optimized sensor design and frequency selection. Findings confirm the efficacy of ECT in differentiating coatings of varying thicknesses and substrate structures, offering a reliable tool for quality control in high-temperature applications.

Keywords Aluminide coating · Eddy current testing · Non-destructive testing · Nickel alloys

1 Introduction

In high-temperature environments, such as those encountered in gas turbines, jet engines, and other aerospace or power generation applications, nickel-based superalloys like MAR-M247 are essential due to their exceptional mechanical strength and resistance to creep and fatigue [1–2]. However, prolonged exposure to elevated temperatures often leads to oxidation and hot corrosion, significantly reducing the lifespan of these materials [3–4]. To enhance their performance and durability, protective coatings such as aluminides are applied. These aluminide coatings form a stable, oxidation-resistant barrier by promoting the formation of a thermally protective alumina layer on the surface [5]. Despite their critical role, the performance of aluminide coatings is highly dependent on their thickness. Coatings that are too thin may fail prematurely, offering insufficient protection, while excessively thick coatings can lead to undesirable stresses and increased weight [1]. Accurate and reliable measurement of coating thickness is therefore essential for quality control during manufacturing and maintenance in service. Traditional methods, such as metallographic cross-sectioning, provide precise measurements but are destructive, time-consuming, and impractical for large-scale or in-service inspections.

✉ Mateusz Kopec
mkopec@ippt.pan.pl

Grzegorz Tytko
grzegorz.tytko@polsl.pl

Małgorzata Adamczyk-Habrajska
malgorzata.adamczyk-habrajska@us.edu.pl

Yong Li
JITRI@xjtlu.edu.cn

Shi Pengpeng
shipengpeng@mail.xjtu.edu.cn

¹ Faculty of Automatic Control, Electronics and Computer Science, Silesian University of Technology, Gliwice 44-100, Poland

² Faculty of Science and Technology, University of Silesia, Chorzów 41-500, Poland

³ State Key Laboratory for Strength and Vibration of Mechanical Structures, Shaanxi Engineering Research Centre of NDT and Structural Integrity Evaluation, Xi'an Jiaotong University, Xi'an, Shaanxi, China

⁴ School of Mathematics and Statistics, Ningxia University, Yinchuan, Ningxia 750021, China

⁵ Institute of Fundamental Technological Research Polish Academy of Sciences, Pawińskiego 5B, Warsaw 02-106, Poland

Eddy current testing (ECT) is a non-destructive evaluation (NDE) technique that has shown great promise for assessing the thickness of coatings, particularly non-magnetic ones like aluminides [6]. The method is based on the interaction between an alternating electromagnetic field generated by a sensor coil and the electrically conductive material being tested. Variations in coating thickness affect the impedance of the eddy current sensor, allowing for indirect measurements of thickness [7–9]. A change in the thickness of the conductive material alters the distribution of the electromagnetic field, which consequently affects the intensity of the induced eddy currents. As a result, the impedance of the eddy current probe is also modified, enabling an indirect measurement of the sample's thickness [10–14]. This process is based on analyzing the measured impedance values corresponding to specific material thicknesses and can be implemented using a calibrated measurement scale. An eddy current sensor can take the form of a single coil [15–18] or consist of several coils working in a receiver-transmitter system [19–22]. Both air-core coils [23–24] and coils with cores of different shapes [25–27] are commonly used. ECT offers several advantages, including speed, sensitivity, and the ability to perform measurements without damaging the component. These attributes make it particularly attractive for industrial applications where efficiency and non-invasiveness are paramount. When applied to aluminide coatings on nickel-based superalloys, ECT presents unique challenges and opportunities. The non-magnetic nature of aluminide coatings, combined with the complex electromagnetic properties of MAR-M247 substrates, requires careful calibration and optimization of the testing parameters. Factors such as the sensor frequency, material conductivity, and surface condition can significantly influence the accuracy and repeatability of measurements [28]. Yong et al. [29] proposed quantitative evaluation of thermal barrier coating based on eddy current technique by using the high-frequency EC excitation coil. The authors stressed, that such coil should operate at high frequency over 3 MHz to enhance the sensitivity of the impedance to the variations in each parameter of thermal barrier coatings (TBCs). Fan and Wang [30] proposed design of eddy current and capacitance dual-mode sensor for thickness detection of thermal barrier coatings which exhibits a sensitivity of $2.67 \text{ m}\Omega \text{ mm}^{-1}$ for bond coating thickness detection in eddy current mode with an excitation frequency of 5 MHz. Li et al. [31] designed a new system based on mutual inductance of Eddy Current System which exhibits the relative errors less than 5% in TBC coating thickness measurements. Since the groundbreaking work by Deeds and Dodd [32], there has been significant development in multi-frequency eddy current techniques. This approach enables compensation for unwanted effects, determination of the probe's optimal

sensitivity, and simultaneous inspections for various depths of eddy current penetration. Numerous intriguing solutions utilizing this method have been developed. Cross-spectral analysis of current and voltage signals using dual digital signal processors (DSP) and fast Fourier transformation (FFT) has enabled signal applications ranging from 1 kHz to 8 MHz [33]. The developed system provided over 250 impedance spectra per second. A highly effective defect classification method based on the spectrum total energy variation was described in [34]. Berneri proposed multi-frequency eddy current testing using a giant magneto-resistance sensor [35]. The presented architecture was implemented on a dedicated instrument whose processing core is a field-programmable gate array (FPGA) for digital signal processing. A novel hybrid serial/parallel multi-frequency measurement method for measuring the impedance of eddy current sensors was studied in [36]. Parallel multi-frequency measurement generally exhibits higher measurement speed but lower signal-to-noise ratio (SNR), whereas serial multi-frequency (sweeping frequency) offers a lower measurement speed but higher SNR. Improvements in inspection accuracy were achieved through the development of a method for determining the lift-off invariant frequency, for which the measured signal is nearly immune to variations in probe lift-off distance [37]. In recent works, multi-frequency eddy current techniques have been integrated with evolutionary algorithms such as multigene genetic programming [38], rotating eddy current [39], and spectrogram eddy current testing [40].

One can note that the recent research on EC methodology in non-magnetic coatings thickness assessment is still expanding, highlighting its importance. According to the authors, the primary challenge in further developing this approach lies in the large number of requirements that must be simultaneously met to achieve the desired inspection effectiveness. The key limitation is the insufficient sensitivity of the eddy current sensor. Consequently, variations in coating thickness on the order of several micrometers often remain undetectable through standard sensor parameter measurements. Furthermore, precise determination of test parameters — including the sensor's operating frequency, accurate calibration of the measurement system for high-frequency precision, and compensation for undesirable factors such as parasitic capacitances, resonance effects, and edge effects — is also required. The novelty of this study lies in the presentation of a measurement technique that meets all these requirements. The developed method enables the detection of small variations in the thickness of thermal barrier coatings (TBC) applied to gas turbine blades, as well as their differentiation based on grain structure. This type of coatings refers to a specialized type of coating designed to insulate and protect components exposed to high temperatures,

particularly in gas turbines, jet engines, and other high-performance machinery. These coatings are typically applied to metal substrates to reduce heat transfer, preventing damage from extreme thermal environments. The inspection is conducted using a custom-designed eddy current sensor featuring a single coil, ensuring the simplest possible construction and the smallest geometric dimensions of the sensor. The introduced design solutions, combined with the use of a pot core, allowed for the desired sensor sensitivity to be achieved. The coil's geometric dimensions were tailored to match the width of the inspected blade, maximizing signal variations while minimizing interference from edge effects. Instead of relying on complex impedance values or phase shift measurements, a direct analysis of resistance variations was introduced. This approach significantly reduced the influence of undesirable factors such as parasitic capacitances. Obtaining accurate results necessitated calibration of the measurement system and precise determination of the sensor's operating frequency. The selected frequency range circumvented resonance effects while ensuring eddy current penetration to a depth corresponding to the coating thickness. Meeting all these conditions enabled the acquisition of significant resistance variations in every conducted test.

2 Materials and methods

Specimens of the MAR 247 nickel-based superalloy, exhibiting three distinct initial microstructures (fine, coarse, and columnar) were manufactured through a standard casting method. These structures were shown in Fig. 1a-c, respectively. The average grain size of these structures was around 0.5 mm, 2.5 mm and 5 mm, respectively. Aluminide coatings were applied via the Chemical Vapor Deposition (CVD) technique. This process was carried out at 1040 °C under a hydrogen-rich atmosphere, with a controlled internal pressure of 150 mbar. Optimized CVD parameters ensured uniform deposition, with durations of 8 h and 12 h resulting in coating thicknesses of 20 μm and 40 μm , as shown in Fig. 1d and e, respectively. An exemplary cross-sectional view of a MAR 247 specimen with a 20 μm coating and performed thickness measurements confirming its uniformity was presented in Fig. 1f-g. Two-layered structure of aluminide coatings includes a uniform region of the β (NiAl) phase secondary solid solution and a heterogeneous NiAl matrix (dark grey) interspersed with Ni_3Al phase precipitates (bright grey) (Fig. 1d-g). Figure 1i shows a technical drawing of a gas turbine blade. All geometric dimensions were determined using a micrometer screw gauge with an accuracy of ± 0.1 mm. Inspection is conducted at the narrowest section of the blade, measuring 15 mm in width and 52 mm in length. The sensor is applied to the sample at an

equidistant position from both of its edges, precisely at the location marked in yellow in Fig. 1c. This is a critical area where stress concentrations lead to blade cracking. The geometric dimensions of this section dictate the size of the eddy current sensor used.

The sensor's diameter should be as large as possible to maximize the inspection range and minimize the influence of interference factors. At the same time, the diameter must be smaller than the width of the inspected area to avoid a dominant edge effect impacting the measurement results. Achieving high sensitivity in a sensor consisting of a single coil requires the use of a pot core, which significantly reduces magnetic flux losses. In the first stage, studies were conducted to determine the optimal outer diameter of the sensor. Three sensors were constructed with core outer diameters of 11 mm, 14 mm, and 18 mm. Based on preliminary measurements performed on sample segments with a width of 25 mm, the largest variations in impedance components were observed for the sensor with an 18 mm diameter, while the smallest variations were recorded for the 11 mm sensor. Subsequently, measurements were conducted for the narrowest section of the sample of 15 mm width. The greatest variations in the sensor's impedance components (i.e. resistance and reactance) were obtained for the 14 mm sensor, while the smallest variations were again measured for the 11 mm sensor. The inferior results obtained for the 18 mm sensor — designated as C18 — indicate a dominant influence of the edge effect.

Initially, the edge effect was examined by incrementally shifting sensor C14 toward one of the lateral edges of the blade in 1 mm steps. Each incremental movement resulted in a reduction of the δR_{MAX} value, which can be attributed to the increasing influence of the blade edge on the sensor's measurements. When sensor C14 was positioned 1 mm from the edge, it was still capable of distinguishing between coatings with thicknesses of 20 μm and 40 μm . However, when placed directly above the blade edge (at a 0 mm distance), the sensor registered identical resistance values for both coatings, making it impossible to differentiate between them. A similar outcome was observed for sensor C18, whose coil's outer diameter is sufficiently large that a pronounced edge effect was detected even when the sensor was displaced by only 1 mm toward the blade edge. In all cases, the sensitivity of the 11 mm sensor was too low to distinguish differences between the tested samples; therefore, it was decided to exclude it from further tests. Unfortunately, for the sample segment with a width of 15 mm, the measured impedance component variations for all sensors were unsatisfactory. For this reason, in the second stage, a modified 14 mm sensor was developed to enhance its sensitivity. The coil was wound using an ultra-thin wire with a cross-section of 0.05 mm to maximize the number of turns.

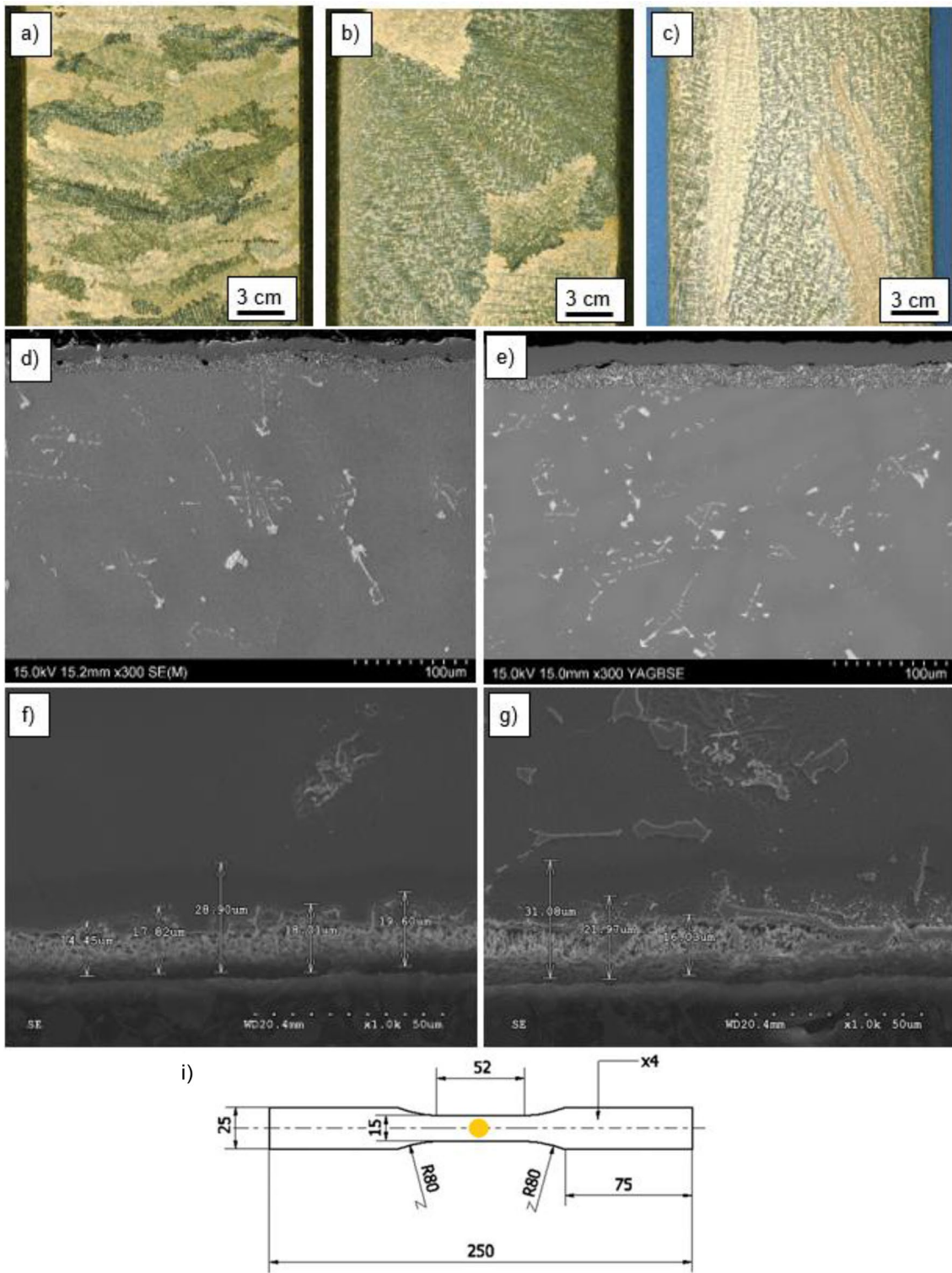


Fig. 1 Initial microstructure of MAR-M247 of fine (a), coarse (b) and column (c) structure. Exemplary cross-sections of the MAR-M247 specimens with 20 μm (d) and 40 μm thick aluminide coatings (e); uni-

formity of coating thickness (f-h). Engineering drawing of the coated specimen with marked area for EC measurements (units in mm) (i)



Fig. 2 Sensor C18 (left), and C14 (right) on sample made of alumide-coated MAR-M247

Table 1 Parameters of the sensors C14 and C18

	C14	C18
Number of turns	740	646
Inner coil radius	3.1 mm	4.3 mm
Outer coil radius	5.5 mm	7.4 mm
Coil height	2.7 mm	4.0 mm
Inner column radius	1.5 mm	1.5 mm
Outer column radius	2.9 mm	3.7 mm
Inner core radius	5.8 mm	7.7 mm
Outer core radius	7.1 mm	9.1 mm
Inner core height	3.0 mm	3.7 mm
Outer core height	4.2 mm	5.3 mm

The winding area was increased by eliminating the coil carcass. The inner surface of the core was coated with a thin layer of adhesive, to which the coil was subsequently fixed. The winding layers were reinforced using Ultifil 2001–815 epoxy resin, which also reduced inter-turn capacitance. The coil leads were soldered using the hot air method to 30 cm long supply wires in such a way as to avoid the formation of a solder joint. The coil, together with the core, was placed inside a sensor head designed to facilitate precise positioning on the tested blade surface. The newly developed sensor was designated as C14 and is shown alongside the C18 sensor in Fig. 2. The parameters of both sensors are presented in Table 1.

The thickness of TBC coatings typically ranges from several tens to several hundred micrometers. In the conducted research, thin coatings with thicknesses of 20 μm and 40 μm were used. The coatings were deposited using the CVD method, achieving a thickness accuracy of $\pm 3 \mu\text{m}$. Investigating structural changes in the coating required selecting an appropriate sensor operating frequency, which determines the penetration depth of eddy currents. A properly chosen frequency ensures that the eddy current penetration depth slightly exceeds the coating thickness. The penetration depth must include the critical bonding layer between the coating and the substrate. Simultaneously, deeper sections of the blade, made of MAR 247 nickel alloy, should not be inspected. Otherwise, the substrate's influence would dominate the results, preventing effective analysis of the thin surface layer.

Measurements were performed using a precision impedance analyzer, Agilent 4294 A, with self-balancing bridge

and an accuracy of $\pm 0.08\%$. Prior to measurements, the analyzer underwent calibration in three modes: open, short, and load. In the load mode, a stable resistor with a resistance value close to that of the tested coil was used. The purpose of calibration is to establish conditions ensuring the specified measurement accuracy by eliminating errors associated with the test instrument.

The sensors were connected to the analyzer using an Agilent measurement fixture and high-quality 16,048 wires supplied by the manufacturer. These wires are specifically matched to the 4294 A device to ensure minimal transmission characteristic losses. Extending the signal path by connecting the sensors can introduce increased measurement errors and imbalance in the bridge circuit. In order to mitigate errors arising from sensor cable connections (50 cm long), a compensation procedure was performed. This process occurs automatically, leveraging the known error characteristics of the 16,048 cables. The analyzer employs advanced internal algorithms to correct the amplitude of the acquired measurement data.

An important aspect of high-frequency testing is the compensation of undesired capacitive effects. When analyzing parameters such as absolute impedance magnitude or phase shift, the influence of parasitic capacitances on measurement results is particularly challenging to eliminate. According to the authors, the commonly employed technique of computing impedance variation as $\Delta Z = Z - Z_0$ is ineffective. This method involves subtracting the baseline impedance Z_0 , measured in the absence of the sample, from the impedance Z obtained during sample testing, thereby aiming to reduce the influence of undesired effects. However, parasitic capacitance affects Z and Z_0 differently, undermining the effectiveness of this approach in high-frequency applications. For these reasons, the authors proposed an alternative method based on sensor resistance measurements, effectively eliminating errors caused by capacitive effects, which predominantly affect the imaginary component of impedance.

The final sensor resistance value was determined as the arithmetic mean of eight measurements taken at 1-second intervals. This calculation was performed using the mathematical function available in the analyzer's software. Averaging the final results helped mitigate random errors that could introduce oscillations in the resistance function plots. Preliminary tests were conducted over a broad frequency range from 1 MHz to 25 MHz. This range starts well above the first resonance frequency, which did not exceed 200 kHz for either sensor. The second resonance frequency was approximately 29 MHz. Due to the significant separation from resonance frequencies, no dynamic impedance component variations due to resonance phenomena were observed within the selected 1 MHz–25 MHz range.

In all cases, the highest sensor sensitivity was observed at frequencies between approximately 11.8 MHz and 12.1 MHz. Identifying this narrow frequency range with the most significant variations in sensor resistance enabled precise measurements at 100 discrete frequency points within the range $f=11.5$ MHz to $f=12.5$ MHz.

3 Results and Discussion

In the first measurement series, blades with a columnar grain structure coated with 20 μm and 40 μm thick layers were used. Measurements were conducted using C14 and C18 sensors to compare their sensitivity and determine whether it is possible to distinguish blades with TBC coatings of different thicknesses. The obtained results are presented in Fig. 3. The resistance values of the C18 sensor for both blades were significantly higher than those of the C14 sensor. However, the largest difference in resistance values for the C14 sensor between the 20 μm and 40 μm coatings was substantially greater than that of the C18 sensor.

To compare the resistance values obtained for the first (R_1) and second (R_2) samples, the absolute resistance difference δR , was defined according to Eq. (1). The maximum δR value obtained across the entire frequency range from 11.5 MHz to 12.5 MHz was designated as δR_{MAX} .

$$\delta R = \left| \frac{R_1 - R_2}{R_1} \right| \cdot 100\% \quad (1)$$

It was assumed that an acceptable δR value should exceed 5% to reliably detect changes in the properties of the tested samples, accounting for the influence of interfering factors and measurement method errors. The reference value

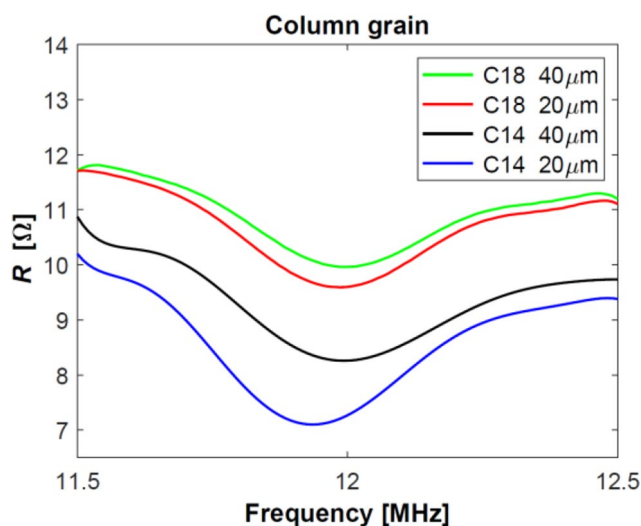


Fig. 3 Resistance R of C14 and C18 sensors for column grain samples with 20 μm and 40 μm thick coatings

R_1 , was defined as the sensor resistance for a blade coated with a 20 μm layer. For the C18 sensor, a δR_{MAX} of approximately 5.7% was obtained. The C14 sensor demonstrated significantly greater sensitivity to changes in coating thickness, achieving a δR_{MAX} of 22.2%. This is a very high value for this parameter, enabling clear differentiation between samples with coating thicknesses of 20 μm and 40 μm . Considering the coating thickness, the maximum difference in sensor resistance values is expected at an inspection depth of approximately 40 μm . At depths less than 20 μm , the structure of both blades is identical, consisting solely of the TBC coating.

In contrast, at depths significantly greater than 40 μm , the dominant influence on the measurement results comes from the MAR-M247 nickel alloy substrate. The δR_{MAX} values were obtained at frequencies of 11.84 MHz (C14) and 11.97 MHz (C18). Given the electrical conductivity of the coatings at 19.5 MS/m, substrate material of 1.2 MS/m and skin effect, the standard penetration depth for eddy currents is approximately 30 μm . At this depth, the eddy current density decreases to about 37% of the surface density. In accordance with the electromagnetic induction phenomenon, when the sensor coil approaches a conductive blade, it induces eddy currents within the material. These currents, in turn, generate a secondary magnetic field which, in line with Lenz's Law, is oriented oppositely to the primary magnetic field produced by the coil. As a consequence, the resultant magnetic field intensity is reduced in comparison to that of the coil alone [41–44]. Furthermore, the magnitude of the induced eddy currents increases with the electrical conductivity of the material. In inspections of very thin layers and coatings, reactance changes are typically too small to distinguish between the tested samples effectively. This is primarily due to the significant impact of undesirable capacitive effects on the imaginary component of impedance. Nevertheless, for both the C14 and C18 sensors, analyses of reactance values were also conducted. However, the results were unsatisfactory. The reactance differences for the C14 sensor did not exceed 2%, while the maximum reactance difference for the C18 sensor was only 0.5%.

In the subsequent measurement series, turbine blades with coarse grain and fine grain substrates, coated with layers of 20 μm and 40 μm thickness, were examined. The results obtained for sensors C14 and C18 are shown in Fig. 4.

Table 2 presents the δR_{MAX} coefficient values for coatings with column, coarse, and fine grain structures. For the C14 sensor, the largest resistance changes were observed for frequencies between 11.84 MHz and 11.89 MHz, while for the C18 sensor, the range was between 11.97 MHz and 12.01 MHz. This narrow frequency range is advantageous for both sensor designers and operators conducting inspections. The minimal variation in the operating frequency

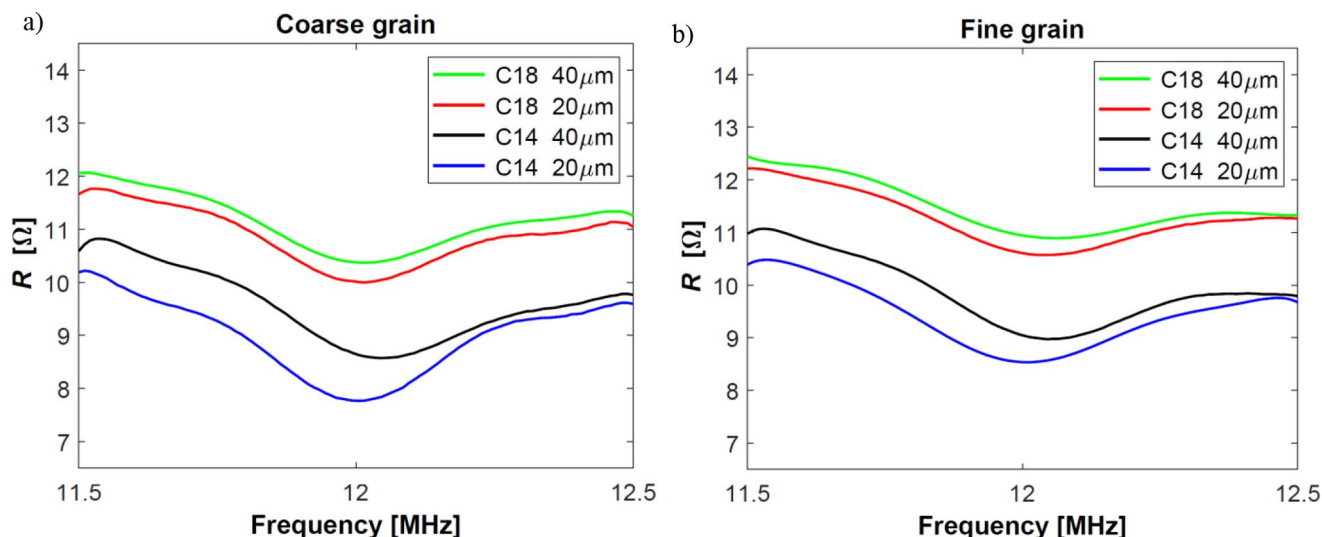


Fig. 4 Resistance R of C14 and C18 sensors for coarse (a) and fine (b) grain samples with 20 μm and 40 μm thick coatings

Table 2 Sensor resistance and δR_{MAX} coefficient values for samples with 20 μm and 40 μm Thick coatings

Probe	Grain structure	Fre-quency [MHz]	R_1 [Ω] 20 μm	R_2 [Ω] 40 μm	δR_{MAX} [%]
C14	Column	11.84	7.46 ± 0.006	9.12 ± 0.007	22.2
C14	Coarse	11.85	8.34 ± 0.007	9.56 ± 0.008	14.6
C14	Fine	11.89	8.74 ± 0.007	9.75 ± 0.008	11.6
C18	Column	11.97	9.61 ± 0.008	10.16 ± 0.008	5.7
C18	Coarse	11.99	10.05 ± 0.008	10.53 ± 0.008	4.8
C18	Fine	12.01	10.60 ± 0.008	11.02 ± 0.009	4.0

values facilitates the determination of optimal measurement system parameters and shortens inspection and result analysis times.

Data in Table 2 clearly indicate that the highest resistance values for the sensors were obtained for the fine grain structure, and the lowest for the column grain. The low δR_{MAX} value for the C18 sensor is due to a very strong edge effect. The coil diameter of this sensor is sufficiently large to induce a “double edge effect,” meaning that both blade edges simultaneously exert a significant influence on the measurement outcome. At the same time, in other tests conducted by the authors for TBC coatings with significantly larger surfaces, the sensitivity of the C18 sensor was greater than that of the C14 sensor.

The largest δR_{MAX} values were obtained for the column grain structure, while the smallest were for the fine grain structure. For the C14 sensor, whose geometry is tailored to the width of the blade fragment being tested, the resistance results allowed for the differentiation of coatings with thicknesses of 20 μm and 40 μm for all three tested structures. Very high δR_{MAX} values, ranging from 12.8 to 22.2%, significantly exceeded the required 5% level. Meanwhile, the sensitivity of the C18 sensor proved to be insufficient, with

δR_{MAX} values between 4% and 5.7%, not providing a clear distinction between the tested blades. As a result, the use of this sensor was abandoned in further tests.

The values of the δR_{MAX} parameter are most influenced by two factors. The first is the interface between the aluminide coating and the MAR-M247 nickel alloy substrate. Different substrate structures lead to varying forms of this interface. The effect of the interface on the sensor’s resistance can be estimated by measuring blades with different substrate structures but the same coating thickness. The second factor is that the depth of eddy current penetration exceeds the thickness of the thinner coating (20 μm), causing the eddy currents to penetrate shallowly into the substrate, whose structure affects the magnetic field distribution and consequently the sensor’s resistance.

Further analysis presents measurement results that allow testing whether eddy current sensors can distinguish samples with coatings of the same thickness but different substrate structures. The resistance values obtained for column, coarse, and fine grain samples with 20 μm coatings are shown in Fig. 5a; Table 3. The measurements were performed using the C14 sensor. In all cases, the obtained δR_{MAX} values were very high. Next, Fig. 5b; Table 3 show the results for 40 μm coatings. The δR_{MAX} values were 3–7% lower than for the 20 μm coatings, but still exceeded the required 5% in all cases. This difference is due to the greater influence of the substrate on the results for thinner coatings, where the depth of eddy current penetration exceeds 20 μm .

C14 and C18 sensors were embedded in the sensor heads to facilitate their positioning along the symmetry axis of the sample (Fig. 1c). Additionally, an analysis of the edge effect on sensor resistance variations was conducted. Due to the complexity of precisely measuring the displacement of the sensor, a numerical model was developed using the Comsol

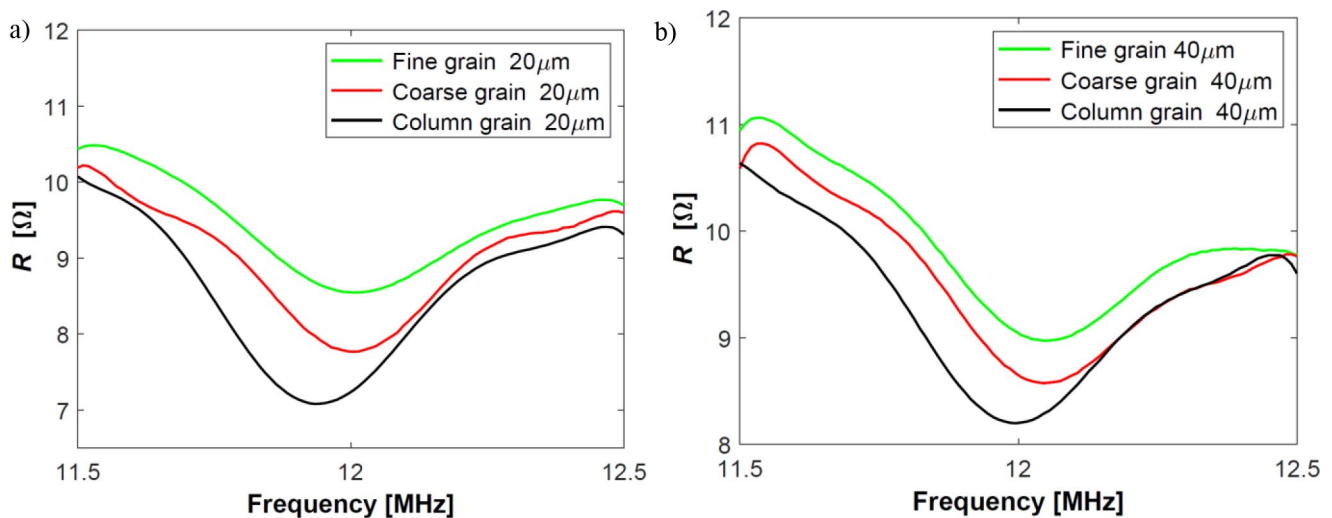


Fig. 5 Resistance R of C14 for samples with 20 μm (a) and 40 μm (b) thick coatings

Table 3 Values of the δR_{MAX} coefficient for samples with 20 μm and 40 μm Thick coatings

Coating thickness	First sample	Second sample	Frequency [MHz]	R_1 [Ω]	R_2 [Ω]	δR_{MAX} [%]
20 μm	Column	Coarse	11.88	7.16 ± 0.006	8.12 ± 0.006	13.5
	Column	Fine	11.84	7.46 ± 0.006	9.05 ± 0.007	21.3
	Coarse	Fine	11.98	7.79 ± 0.006	8.59 ± 0.007	10.3
40 μm	Column	Coarse	11.91	8.33 ± 0.007	9.19 ± 0.007	10.3
	Column	Fine	11.94	8.21 ± 0.007	9.33 ± 0.007	13.6
	Coarse	Fine	12.02	8.50 ± 0.007	9.11 ± 0.007	7.2

Multiphysics software package. Computer simulations were performed using the finite element method (FEM), with the solution domain discretized into approximately 60,000 triangular elements. Based on the obtained results, the optimal outer coil radius was determined to be 5.8 mm (whereas in the applied C14 sensor, this parameter was 5.5 mm). Under these conditions, the most significant differences in resistance values were observed for blades with coatings of 20 μm and 40 μm thickness. The distance from the blade edge at which a gradual decrease in δR_{MAX} was noted was 1.8 mm. For distances below 0.5 mm, resistance variations were too small to distinguish between blades with different coating thicknesses due to the dominant influence of the edge effect.

One should note that the morphology of the microstructure, particularly grain size and geometry, has a pronounced influence on magnetic permeability and, to a lesser extent, electrical resistivity. In ferromagnetic materials such as MAR-M247 nickel-based superalloy, magnetic permeability is significantly affected by domain wall movement. Grain boundaries act as pinning sites that impede the motion of magnetic domain walls. Therefore, microstructures with finer grains, such as the one shown in Fig. 1a (average grain size ~ 0.5 mm), have a higher grain boundary density, which leads to increased domain wall pinning and consequently lower magnetic permeability. In contrast, the coarse

(Fig. 1b, ~ 2.5 mm) and columnar (Fig. 1c, ~ 5 mm) grain structures exhibit lower boundary density, allowing domain walls to move more freely and thus resulting in higher permeability. This relationship between grain boundary density and domain wall mobility is well-established in magnetic materials research [45–47]. While electrical resistivity is less sensitive to grain size compared to magnetic permeability, it can still be influenced by increased electron scattering at grain boundaries in finer-grained materials. This results in slightly higher resistivity, although the magnitude of this effect is typically modest [48]. On the other hand, coating thickness predominantly affects the signal through the lift-off effect. As the non-conductive coating increases in thickness, the distance between the sensor and the conductive substrate increases, reducing eddy current coupling and altering the sensor impedance. However, variations in substrate microstructure—specifically magnetic permeability changes due to different grain morphologies—also impact the eddy current response, but through a different physical mechanism. Changes in permeability affect the skin depth and magnetic field distribution, thereby modifying the signal decay and amplitude in ways distinct from the geometric lift-off effect. This dual influence—lift-off for coatings and permeability for microstructure—is well documented in the literature [49].

The developed method's ability to detect subtle variations in thermal TBC thickness and distinguish differences in grain structure is attributed to the distinct influences these factors have on the distribution of induced magnetic fields and the resultant eddy current responses. Grain structure affects local magnetic field distributions due to variations in electrical conductivity and magnetic permeability at the microstructural level [50]. Coarse-grained TBCs exhibit different eddy current densities compared to fine-grained ones, leading to measurable variations in impedance [51]. However, these grain structure-induced impedance changes are significantly smaller than those caused by variations in coating thickness, which produce more pronounced modulations of eddy current paths and signal amplitude [52]. While grain boundary pinning of domain walls influences magnetic properties such as coercivity and susceptibility, this effect is more prominent in ferromagnetic materials [53]. Since many TBCs are non-ferromagnetic or weakly magnetic, the impact of domain wall movement on impedance is generally minimal in this context. To reliably separate the effects of grain structure and thickness in signal interpretation, one can exploit the relative magnitude of the impedance variations. Thickness changes induce larger shifts in both the real and imaginary components of impedance, enabling straightforward differentiation from the finer-scale variations caused by grain morphology [51, 52]. Furthermore, employing multi-frequency or multi-modal eddy current measurements can enhance selectivity, as thickness and microstructure influence the frequency-dependent response differently, allowing for more robust discrimination between these two effects [51, 53].

The thickness of the thermal barrier coatings employed in practical applications as protective layers for gas turbine blades typically ranges from 20 μm to 500 μm . The sensitivity of a standard eddy current probe enables the successful inspection of thicker coatings (above 200 μm). In the present study, measurements were carried out for coatings with thicknesses as low as 20 μm and 40 μm . These measurements require the application of a probe characterized by high sensitivity and geometry tailored to the dimensions and shape of the sample under examination. The obtained results confirm that the presented measurement technique can be applied to coatings on gas turbine blades with a thickness of 20 μm . One should mention, that even thinner coatings (below 20 μm) could be investigated if a probe with a higher operational frequency signal will be used. The measurements confirmed that eddy current inspections using the designed sensor can differentiate gas turbine blades made from substrates with different structures and containing coatings of different thicknesses. The analysis of the obtained measurement results led to the following conclusions:

- Optimized sensor design and proper selection of the sensor's geometric dimensions allows for achieving the required sensitivity for testing coatings and thin layers. Very good results were obtained in the resistance measurements. However, the changes in reactance values were insufficient for effectively distinguishing the tested samples.
- The frequencies at which the δR parameter reached its highest value were in the range of 11.84 MHz to 12.02 MHz. Such a small variation in the optimal operating frequency of about 1.5% enables efficient measurement and analysis of the results.
- The highest sensitivity of the sensor was achieved for the standard depth of penetration of approximately 30 μm . At this depth, the eddy current density decreases to about 37%, and at a depth of 60 μm , it drops to 13.5%. The optimal operating frequency of the sensor, and consequently the penetration depth, depends on the thickness of the layers being tested, which in these measurements were 20 μm and 40 μm .
- The δR_{MAX} values were higher for the 20 μm coated samples compared to those with 40 μm coatings. This indicates that blades with 20 μm coatings are easier to differentiate using the proposed method.
- When comparing the samples with 20 μm and 40 μm coatings, the greatest difference in resistance values was obtained for the column substrate structure, and the smallest for the fine structure.
- The edge effect has such a significant impact on the sensor's resistance values that the optimal coil diameter should be slightly smaller than the width of the blade section being tested. This size also facilitates precise sensor positioning relative to the sample.

4 Conclusions

The study demonstrates that ECT is an effective non-destructive technique for evaluating the thickness and structural variations of non-magnetic aluminide coatings on MAR-M247 nickel-based superalloy. The C14 sensor, optimized for construction and blade geometry, exhibited superior sensitivity compared to the larger C18 sensor, enabling clear differentiation of coatings with thicknesses of 20 μm and 40 μm as well as various substrate grain structures. The narrow optimal frequency range (11.84 MHz to 12.02 MHz) ensures reliable and efficient measurements, while the impact of penetration depth emphasizes the importance of coating thickness and substrate influence. The findings confirm ECT's utility in distinguishing coatings or substrates, offering a precise and non-invasive solution for quality control in high-temperature applications, particularly in the

aerospace and energy sectors. The constant blade width at the inspection site (15 mm) facilitates the optimization of the testing process by implementing solutions commonly used in turbine inspections. The sensor can be positioned either within a dedicated test fixture attached to the blade or within a specialized holder. Both methods ensure precise alignment of the sensor along the blade's axis of symmetry, maintaining an equal distance from both blade edges. Furthermore, both the fixture and the holder provide positional stabilization of the sensor, minimizing the risk of tilting and reducing the lift-off effect.

Acknowledgements The authors would like to express their gratitude to Mr M. Wyszowski and Prof. D. Kukla for their kind help during the experimental part of this work.

Author Contributions Grzegorz Tytko: Conceptualization, Data curation, Formal analysis, Investigation, Methodology, Project administration, Supervision, Validation, Visualization, Roles/Writing - original draft, Writing - review & editing. Małgorzata Adamczyk-Habrajska: Data curation, Investigation, Validation. Yong Li: Formal analysis, Methodology, Writing - review & editing. Zenghua Liu: Formal analysis, Methodology, Writing - review & editing. Mateusz Kopec: Conceptualization, Data curation, Formal analysis, Investigation, Methodology, Project administration, Supervision, Validation, Visualization, Roles/Writing - original draft, Writing - review & editing.

Data Availability No datasets were generated or analysed during the current study.

Declarations

Competing Interests The authors declare no competing interests.

Open Access This article is licensed under a Creative Commons Attribution 4.0 International License, which permits use, sharing, adaptation, distribution and reproduction in any medium or format, as long as you give appropriate credit to the original author(s) and the source, provide a link to the Creative Commons licence, and indicate if changes were made. The images or other third party material in this article are included in the article's Creative Commons licence, unless indicated otherwise in a credit line to the material. If material is not included in the article's Creative Commons licence and your intended use is not permitted by statutory regulation or exceeds the permitted use, you will need to obtain permission directly from the copyright holder. To view a copy of this licence, visit <http://creativecommons.org/licenses/by/4.0/>.

References

- Kopec, M.: Effect of aluminide coating thickness on High-Temperature fatigue response of MAR-M247 Nickel-Based Superalloy. *Coatings*. **14**, 1072 (2024). <https://doi.org/10.3390/coatings14081072>
- Šulák, I., Obrtlík, K.: AFM, SEM AND TEM study of damage mechanisms in cyclically strained mar-M247 at room temperature and high temperatures. *Theoret. Appl. Fract. Mech.* **108**, 102606 (2020). <https://doi.org/10.1016/j.tafmec.2020.102606>
- Šulák, I., Obrtlík, K., Čelko, L., et al.: High-Temperature Low-Cycle fatigue behaviour of MAR-M247 coated with newly developed thermal and environmental barrier coating. *Adv. Mater. Sci. Eng.* 9014975 (2018). <https://doi.org/10.1155/2018/9014975>
- Šulák, I., Obrtlík, K.: Thermomechanical and isothermal fatigue properties of MAR-M247 Superalloy. *Theoret. Appl. Fract. Mech.* **131**, 104443 (2024). <https://doi.org/10.1016/j.tafmec.2024.104443>
- Kopec, M.: Recent Advances in the Deposition of Aluminide Coatings on Nickel-Based Superalloys: A Synthetic Review (2019–2023). *Coatings*. vol. 14, no. 5, 630. (2024). <https://doi.org/10.3390/coatings14050630>
- Tytko, G., Adamczyk-Habrajska, M., Luo, Y., et al.: Eddy current testing in the quantitative assessment of degradation state in MAR247 nickel Superalloy with aluminide coatings. *J. Nondestr. Eval.* **43**(4), 112 (2024). <https://doi.org/10.1007/s10921-024-01129-x>
- Cao, B., Sun, J., Fan, M., et al.: Novel conductivity measurement of thin metallic materials using crossover frequency feature from Triple-Frequency eddy current signals. *IEEE Trans. Instrum. Meas.* **73**, 6005611 (2024). <https://doi.org/10.1109/TIM.2024.3383059>
- Huang, P., Pu, H., Li, J., et al.: An eddy current testing method for thickness and conductivity measurement of Non-Magnetic material. *IEEE Sens. J.* **23**(5), 4445–4454 (2023)
- Goruleva, L.S., Skorynina, P.A., Savrai, R.A.: Application of magnetic and Eddy-Current methods to assess the thickness of the hardened layer on the surface of AISI 321 metastable austenitic steel subjected to frictional treatment. *J. Nondestr. Eval.* **44**(11) (2025). <https://doi.org/10.1007/s10921-024-01150-0>
- Abdou, A., Bouchala, T., Abdelhadi, B., et al.: Nondestructive eddy current measurement of coating thickness of aeronautical construction materials. *Instrum. Mesure Métrologie.* **18**(5), 451–457 (2019). <https://doi.org/10.18280/i2m.180504>
- Sardellitti, A., Milano, F., Laracca, M., et al.: An eddy-current testing method for measuring the thickness of metallic plates. *IEEE Trans. Instrum. Meas.* **72**, 1–10 (2023)
- Wang, D., Xu, J., Xin, W., et al.: Thickness and conductivity measurement of nonferromagnetic metal coating using apparent eddy current conductivity. *IEEE Trans. Instrum. Meas.* **73**, 1–10 (2024). <https://doi.org/10.1109/TIM.2024.3427749>
- Lin, C.-Y., Huang, R.-Y., Teng, M., et al.: Pulsed eddy current sensor for cascade electrical conductivity and thickness Estimation in nonferrous metal plates. *IEEE Sens. J.* **23**(8), 8323–8334 (2023)
- Wang, W., Zhang, Z., Yin, W., et al.: Nonmagnetic metal plate thickness measurement algorithm based on inductance imaginary part slope. *IEEE Sens. J.* **24**(15), 23658–23666 (2024)
- Tytko, G.: Locating defects in conductive materials using the eddy current model of the filamentary coil. *J. Nondestr. Eval.* **40**(3), 66 (2021)
- Zhang, S.: Analytical model of an I-core coil for nondestructive evaluation of a conducting cylinder below an infinite plane conductor. *Meas. Sci. Rev.* **21**(4), 99–105 (2021)
- Tytko, G., Dziezkowski, L., Magnuski, M., et al.: Eddy current testing of conductive discs using the pot-core sensor. *Sens. Actuators A: Phys.* **349**, 114060 (2023)
- Tytko, G.: Locating defects in conductive materials using the eddy current model of the filamentary coil. *J. Nondestruct Eval.* **40**, 66 (2021). <https://doi.org/10.1007/s10921-021-00798-2>
- Yu, D., Chen, B., Luo, Y., et al.: Mutual inductance calculation for rectangular and circular coils with parallel axes. *IET Electr. Power Appl.* **18**(4), 379 (2023). <https://doi.org/10.1049/elp2.12396>
- Wang, R., Bao, B., Wang, W., et al.: Research on Remote-Field eddy current focusing method for detecting hidden defects in

- aircraft riveted components. *J. Nondestr. Eval.* **42**(95) (2023). <https://doi.org/10.1007/s10921-023-01011-2>
21. Xu, Z., Zhu, C., Jin, J., et al.: Reduction of pulsed eddy current probe footprint using sequentially excited multiple coils. *J. Nondestr. Eval.* **43**(47) (2024). <https://doi.org/10.1007/s10921-024-01072-x>
 22. Yidan, Z., Zou, H., Li, Z., et al.: The image classification method for eddy current inspection of titanium alloy plate based on parallel sparse filtering and deep forest. *J. Nondestr. Eval.* **43**(103) (2024). <https://doi.org/10.1007/s10921-024-01069-6>
 23. Xia, Z., Yan, J., Huang, R., et al.: Fast Estimation of metallic pipe properties using simplified analytical solution in Eddy-Current testing. *IEEE Trans. Instrum. Meas.* **72**, 1000513doi (2023). <https://doi.org/10.1109/TIM.2022.3224516>
 24. Deng, Z., Wang, Y., Shi, Q., et al.: 2-D analytical model of sinusoidal eddy current field based on permeability distortion. *IEEE Sens. J.* **24**(9), 14392 (2024). <https://doi.org/10.1109/JSEN.2024.3376804>
 25. Tytko, G., Dzikowski, L.: Calculation of the impedance of an E-cored coil placed above a conductive material with a surface hole. *Meas. Sci. Rev.* **19**(2), 43–47 (2019)
 26. Zhang, S.: Investigation of flux transfer along ferrite core of probe coil for eddy current nondestructive evaluation. *Meas. Sci. Rev.* **23**(1), 11–18 (2023)
 27. Cui, L., Zeng, Z., Jiao, S.: Finite element analysis of eddy current testing of aluminum honeycomb sandwich structure with CFRP panels based on the domain decomposition method. *J. Nondestr. Eval.* **43**(44) (2024). <https://doi.org/10.1007/s10921-024-01053-0>
 28. Machado, M.A.: Eddy currents probe design for NDT applications: A review. *Sensors.* **24**, 5819 (2024). <https://doi.org/10.3390/s24175819>
 29. Yong, L., Chen, Z., Mao, Y., et al.: Quantitative evaluation of thermal barrier coating based on eddy current technique, *NDT & E International*, vol. 50, pp. 29–35, (2012). <https://doi.org/10.1016/j.ndteint.2012.04.006>
 30. Fan, W., Wang, L.: Design of eddy current and capacitance dual-mode sensor for thickness detection of thermal barrier coatings. *Meas. Sci. Technol.* **35**(12), 125119 (2024)
 31. Li, C., Fan, M., Cao, B., et al.: Thickness measurement of thermal barrier coating based on mutual inductance of eddy current system. *IEEE Trans. Industr. Electron.* **71**(7), 8099–8109 (2024)
 32. Deeds, W.E., Dodd, C.V., Scott, G.W.: Computer-aided design of multifrequency eddy-current tests for layered conductors with multiple property variations (No. ORNL/TM-6858). (1979). Oak Ridge National Lab.(ORNL), Oak Ridge, TN (United States)
 33. Yin, W., Dickinson, S.J., Peyton, A.J.: A multi-frequency impedance analysing instrument for eddy current testing. *Meas. Sci. Technol.*, **17**, 2, (2006)
 34. Gao, J., Pan, M., Luo, F.: Defect identification and classification of multi-frequency eddy current test based on spectrum method. The 2010 IEEE International Conference on Information and Automation, Harbin, China, 2010, pp. 1883–1886. <https://doi.org/10.1109/ICINFA.2010.5512024>
 35. Bernieri, A., Betta, G., Ferrigno, L., et al.: Multi-frequency eddy current testing using a GMR based instrument. *Int. J. Appl. Electromagnet Mech.* **39**, 355–362 (2012). <https://doi.org/10.3233/JAE-2012-1482>
 36. Chen, Z., Salas-Avliá, J.R., Tao, Y., et al.: A novel hybrid serial/parallel multi-frequency measurement method for impedance analysis in eddy current testing. *Rev. Sci. Instrum.* **91**(2) (2020). <https://doi.org/10.1063/1.5130734>
 37. Lu, M., Meng, X., Huang, R., et al.: Lift-off invariant inductance of steels in multi-frequency eddy-current testing. *NDT E Int.* **121**, 102458 (2021). <https://doi.org/10.1016/j.ndteint.2021.102458>
 38. Ge, J., Yusa, N., Fan, M.: Frequency Component Mixing of Pulsed or multi-frequency Eddy Current Testing for Nonferromagnetic Plate Thickness Measurement Using a multi-gene Genetic Programming Algorithm, vol. 120, p. 102423. *NDT & E International* (2021). <https://doi.org/10.1016/j.ndteint.2021.102423>
 39. Carere, F., Sangiovanni, S., Laracca, M., et al.: Improving Defect Detection in Eddy Current Testing using Multi-Frequency Rotating Eddy Current Strategy. In 2024 11th International Workshop on Metrology for AeroSpace (MetroAeroSpace), pp. 123–127. IEEE. (2024)
 40. Grochowalski, J.M., Chady, T.: Pulsed Multifrequency Excitation and Spectrogram Eddy Current Testing (PMFES-ECT) for Non-destructive Evaluation of Conducting Materials. *Materials*, vol. 14, no. 18, 5311. (2021). <https://doi.org/10.3390/ma14185311>
 41. Harms, J., Kern, T.A.: Theory and modeling of Eddy current type inductive conductivity sensors. *Engineering proceedings*, vol. 6, no. 1, p. 37. (2021)
 42. Xia, Z., Huang, R., Chen, Z., et al.: Eddy current measurement for planar structures. *Sensors*, vol. 22, no. 22, p. 8695. (2022)
 43. Salon, S.J., Chari, M.V., Ergene, L.T., et al.: *Eddy Currents: Theory, Modeling, and Applications*. Wiley (2023)
 44. Romero-Arismendi, N.O., Olivares-Galvan, J.C., Hernandez-Avila, J.L., et al.: Past, present, and future of new applications in utilization of eddy currents. *Technologies*, vol. 12, no. 4, p. 50. (2024)
 45. Cullity, B.D., Graham, C.D.: *Introduction To Magnetic Materials*. Wiley (2011)
 46. Bozorth, R.M.: *Ferromagnetism*. IEEE, (1993)
 47. Herzer, G.: Grain size dependence of coercivity and permeability in nanocrystalline ferromagnets. *IEEE Trans. Magn.* **26**(5), 1397–1402 (1990)
 48. Mott, N.F., Davis, E.A.: *Electronic Processes in Non-Crystalline Materials*. Oxford University Press (1979)
 49. Tian, G.Y., Sophian, A.: Reduction of Lift-Off Effects for Pulsed Eddy Current NDT, vol. 38, pp. 319–324. *NDT & E International* (2005). 4
 50. Gómez-García, J., Rico, A., Garrido-Maneiro, M.A., Múnez, C.J., Poza, P., Utrilla, V.: Correlation of mechanical properties and electrochemical impedance spectroscopy analysis of thermal barrier coatings. *Surf. Coat. Technol.* **204**, 6–7 (2010). <https://doi.org/10.1016/j.surfcoat.2009.09.064>
 51. Li, Y., Yan, B., Li, W., Li, D.: Thickness assessment of thermal barrier coatings of aeroengine blades via dual-frequency eddy current evaluation. *IEEE Magn. Lett.* **7**, 1304905 (2016). <https://doi.org/10.1109/LMAG.2016.2587740>
 52. Sabbagh, H.A., Knopp, J.S., Aldrin, J.C., Murphy, R.K., Sabbagh, E.H.: Eddy current inversion and estimation metrics for evaluating thermal barrier coatings. *AIP Conference Proceedings*, vol. 1211, no. 1, pp. 703–710. (2010). <https://doi.org/10.1063/1.3362463>
 53. Colaiori, F., Durin, G., Zapperi, S.: Eddy current damping of a moving domain wall: Beyond the quasistatic approximation. *Phys. Rev. B.* **76**, 224416 (2007). <https://doi.org/10.1103/PhysRevB.76.224416>